Article

Structure

Structural insights into human ABCA7-mediated lipid transport

Graphical abstract

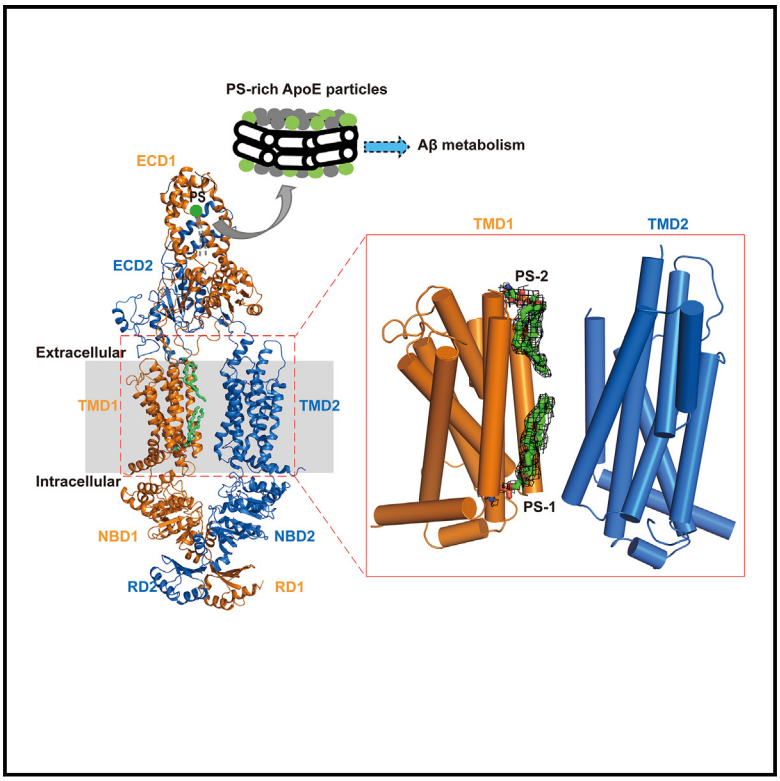

Authors

Shu-Cheng Fang, Liang Wang, Meng-Ting Cheng, ..., Cong-Zhao Zhou, Wen-Tao Hou, Yuxing Chen

Correspondence

zcz@mail.ustc.edu.cn (C.-Z.Z.), todvince@mail.ustc.edu.cn (W.-T.H.), cyxing@ustc.edu.cn (Y.C.)

In brief

Fang et al. determined two cryo-EM structures of ABCA7 in the apo and substrate-bound states, respectively and revealed that ApoE interacts with ABCA7, which significantly enhances its activities. These findings not only provide structural insights into ABCA7-mediated PS translocation, but also reveal a potential mechanism for ApoE-related Alzheimer's disease onset.

Highlights

- 3.5 Å cryo-EM structure of human ABCA7 in the substrate-bound form
- Two phosphatidylserine molecules bind to TMD1 in a unique "tail-to-tail" manner
- ApoE interacts with ABCA7 and influences the lipid transport activity of ABCA7
- Activity assay results for ABCA7 clinical mutations are correlated with AD onset data

Fang et al., 2025, Structure *33*, 1–11
March 6, 2025
https://doi.org/10.1016/j.str.2024.12.015

CellPress

Structure

CellPress

Article

Structural insights into human ABCA7-mediated lipid transport

Shu-Cheng Fang,[1,2] Liang Wang,[1,2] Meng-Ting Cheng,[1,2] Da Xu,[1,2] Zhi-Peng Chen,[1,2] Jie Wang,[1,2] Wenli Liao,[3] Yanyan Li,[3] Cong-Zhao Zhou,[1,2,*] Wen-Tao Hou,[1,2,*] and Yuxing Chen[1,2,4,*]

[1]Department of Endocrinology, Institute of Endocrine and Metabolic Diseases, The First Affiliated Hospital of USTC, and Center for Advanced Interdisciplinary Science and Biomedicine of IHM, Division of Life Sciences and Medicine, University of Science and Technology of China, Hefei 230027, China

[2]Biomedical Sciences and Health Laboratory of Anhui Province, University of Science and Technology of China, Hefei 230027, China

[3]Institute for Biological Electron Microscopy, Southern University of Science and Technology, Shenzhen 518055, Guangdong, China

[4]Lead contact

*Correspondence: zcz@mail.ustc.edu.cn (C.-Z.Z.), todvince@mail.ustc.edu.cn (W.-T.H.), cyxing@ustc.edu.cn (Y.C.)

https://doi.org/10.1016/j.str.2024.12.015

SUMMARY

The human ATP-binding cassette (ABC) transporter ABCA7 participates in the lipidation of apolipoprotein ApoE, a commonly recognized risk factor for Alzheimer's disease (AD). How ABCA7 is involved in the molecular pathogenesis of AD remains poorly understood. Using cryoelectron microscopy (cryo-EM), we determined ABCA7 structures in the apo and substrate-bound forms, respectively. Combined with activity assays, we assigned the residues that specifically bind two molecules of phosphatidylserine (PS) that are arranged in a "tail-to-tail" manner. Pull-down assays confirmed that ApoE directly interacts with ABCA7; and moreover, both ATPase and lipid transport activities of ABCA7 were significantly enhanced in the presence of ApoE. We also measured the activities of a familial AD variant and a protective clinically reported variant in the ABCA7 gene. Our findings not only give structural insights into ABCA7-mediated PS translocation, but we also provide first biochemical evidence for its link to AD by forwarding lipids to ApoE.

INTRODUCTION

Alzheimer's disease (AD) is an irremediable neurodegenerative disease that primarily affects the brain, causing memory loss and cognitive disabilities.[1] AD accounts for 60%–80% dementia cases, which not only suffers the patients but also places a significant burden on their families and caregivers.[2] AD patients are diagnosed by the accumulation of abnormal protein deposits in the brain, known as amyloid β (Aβ) plaques and tau tangles, which disrupt normal functioning of brain cells.[1,3] However, the pathogenesis of AD is still poorly understood, although many risk factors are reported, including environmental[4–7] and genetic factors.[1,8–11] Among the genetic risk factors, *APOE* is widely believed as a major gene that is associated with aggregation, clearance, cellular uptake of Aβ and also affects synapse number and function, blood brain barrier integrity and Tau-mediated neurodegeneration.[12–14]

ApoE is a ubiquitous lipid carrier that forms lipoprotein particles via binding to a variety of lipid species including phospholipids, triglycerides (TAGs) and cholesterol.[15,16] It is the major apolipoprotein expressed in the central nervous system, which binds to the low-density lipoprotein receptors (LDLRs), mediating the cellular uptake and lysosomal hydrolysis of lipids.[17–20] A recent study reported that the decreased binding affinity of ApoE to the receptors, such as HSPG (heparan sulfate proteoglycan core protein) and LRP1 (low-density lipoprotein receptor-related protein 1), was linked to the impeded process of Aβ-induced tau seeding and spreading *in vivo*, subsequently resulting in a protective effect against AD onset.[21] In fact, the ApoE lipoprotein particles of higher PS abundancy were reported to attribute to a weaker binding affinity toward LRP1.[22] In the process of ApoE lipidation, two members from the A family of human ATP-binding cassette (ABC) superfamily, ABCA1 and ABCA7 are involved.[23,24] It has been suggested that ABCA1 is mainly responsible for the cholesterol delivery, whereas ABCA7 presents phospholipids to ApoE.[25] Of note, ABCA7, the coding gene of which shares a same chromosomal location with that of ApoE, has been shown a significant correlation with AD, based on diverse genome-wide association studies (GWAS) of AD patients worldwide.[11,26] A series of clinic reports have denoted that the presence of single nucleotide polymorphisms, missense variants, premature termination codon variants and protein modifications on ABCA7 or its gene has a robust association with AD patients.[27–29] It has been proposed that ABCA7 can regulate the physiological processes related to Aβ metabolism via affecting ApoE lipidation,[1,24,25,30] yet no direct evidence reported so far.

ABCA7 is a polypeptide of 2,146 residues, folded into two transmembrane domains (TMDs) with each consisting of six transmembrane helices (TMs) and two nucleotide-binding

Please cite this article in press as: Fang et al., Structural insights into human ABCA7-mediated lipid transport, Structure (2024), https://doi.org/10.1016/j.str.2024.12.015

domains (NBDs). In addition, ABCA7 also possesses two typical structure features in ABCA family members,[31,32] including a large extracellular domain (ECD) inserted between TM1 and TM2, and a small regulatory domain (RD) succeeding each NBD (Figure S1A). ABCA7 is expressed in neurons, astrocytes, microglia, endothelial cells of the blood-brain barrier and brain pericytes.[32] Previous reports showed that ABCA7 can transfer phospholipids, such as phosphatidylserine (PS), phosphatidylcholine (PC), phosphatidylethanolamine (PE), and sphingomyelin (SM), to apolipoproteins, usually ApoE or ApoA-I.[24,33] Although the cryoelectron microscopy (cryo-EM) structures of ABCA7 in apo and ATP-bound states have been recently reported,[34] the substrate-binding pattern and transport mechanism remain unknown.

Here we report the cryo-EM structures of human ABCA7 in apo form at 3.9 Å and substrate-bound form at 3.5 Å. Structural analysis combined with biochemical assays suggested a lipid transport mechanism of ABCA7. Remarkably, we found the direct interaction between ApoE and ABCA7 and further revealed that the transport and ATPase activities of ABCA7 could be enhanced in the presence of ApoE. Finally, our data imply an underlying mechanism of ApoE-related AD onset.

RESULTS

Biochemical characterization and structure determination of ABCA7

The full-length human *ABCA7* was recombinantly expressed in human embryonic kidney HEK293 cells and purified to homogeneity in detergent micelles. The ABCA7 protein was extracted from the membrane with detergent n-dodecyl-β-D-maltoside (DDM) plus cholesteryl hemisuccinate (CHS) and exchanged to glyco-diosgenin (GDN) during purification (Figure S1B). The purified wild-type (WT) ABCA7 displayed an ATPase activity with K_m and V_{max} values of 465 μM and 5.66 mol Pi min^{-1} mol^{-1} protein, respectively (Figure 1A), which is comparable with previously reported ABCA transporters (Table S1). ABCA7 possesses two ATPase catalytic sites, Glu965 and Glu1951, in NBD1 and NBD2, respectively. We thus mutated these two Glu to Gln (Figure S1C) and found that E965Q/E1951Q mutant exhibited an almost abolished ATP hydrolysis activity (Figure 1A). We further performed substrate-stimulated ATPase activity assays with putative substrates of ABCA7 suggested in the previous studies.[25,33,35] Compared to the basal ATPase activity of ABCA7, dioleoylphosphatidylcholine (DOPC), and dioleoylphosphatidylethanolamine (DOPE) displayed no significant stimulation of activity (Figure 1B); however, the ATPase activity was increased ~2-folds upon the addition of dioleoylphosphatidylserine (DOPS, Figure S1D). In addition, the proteoliposome-based transport assays revealed that the transport activity of ABCA7 toward the fluorescence-labeled PS is also significantly higher than PE and PC (Figures S1E–S1G). To study whether PS with differing chain lengths and double bond positions would possess different stimulated ATPase activities, we performed the assays of several different types of PS, which showed similar activities and all are significantly higher than DOPC and DOPE (Figures 1B and S1D). The result indicated that the polar heads of phospholipids might play a more important role in the substrate specificity of ABCA7. A further concentration-dependent DOPS-stimulated ATPase activity assay revealed a half maximal effective concentration (EC_{50}) value of 209 μM and a V_{max} of 12.08 mol Pi min^{-1} mol^{-1} protein (Figure 1C). The results of these biochemical assays indicated that our protein samples are in a physiologically relevant state, and that PS might be the most preferable substrate of ABCA7.

To gain more structural and functional insights into ABCA7, we first solved the apo-form structure with the $ABCA7_{E965Q/E1951Q}$ variant samples using cryo-EM, at the resolution of 3.9 Å (Figure S2; Table S2). The structure adopts an outward-facing (OF) conformation (Figure 1D). The NBDs possess a classic NBD fold of ABC transporter, with an α-helical subdomain and a RecA-like ATPase core subdomain. The TMDs of ABCA7 exhibit a typical type-V ABC exporter fold without TM swapping.[36] Each of the two TMDs consists of 6 TMs and contact with each other in the cytoplasmic membrane leaflet through a small interface between TM5 and TM11. Two intercellular helices (IH2 and IH4) insert the NBD of the same side and couple conformational changes between the two domains (thus also named coupling helices, Figures 1D and S1A). The two RDs adopt domain swapping to interact with their opposite NBDs, respectively. Of note, the resolution of TMD1 is much higher than TMD2 (Figure S2B).

ABCA7 possesses two extracellular domains, ECD1 and ECD2, which are inserted in TMD1 and TMD2 (between TM1 and TM2 in TMD1, and TM7 and TM8 in TMD2), respectively (Figures 1D and S1A). These two ECDs co-twist as one torch-like structure (Figure 1E), generally similar to the previously reported ECDs in ABCA1[37] and ABCA4.[38] Specifically, ECD1 consists of 15 α-helices and 8 β-strands, while ECD2 contains 6 α-helices and 8 β-strands (Figures 1E and S3A). Different from the ECDs of ABCA1 or ABCA4 which are divided into three layers: the base, the tunnel and the lid, the ECDs of ABCA7 only consist of the base of two α/β domains from ECD1 and ECD2 and the tunnel primarily formed by α helices from ECD1 in addition to an α-helical hairpin from ECD2, but not the lid (Figures 1E and S3B). In fact, sequence alignment also revealed that the sequence corresponding to the lid is missing in ECD1 of ABCA7 (Figure S3C).

The substrate-bound structure revealed two PS molecules binding to TMD1 side of the translocation cavity in a tail-to-tail manner

We prepared the WT ABCA7 samples and solved the structure at the resolution of 3.5 Å (Figures 2A and S4; Table S2). In the translocation cavity between TMD1 and TMD2, two extra densities could be found proximal to the TMD1 (Figures 2B and S4F), similar densities at the counterpart position found in a previously reported structure of ABCA7.[34] However, only the acyl chains could be fitted into the densities due to the poor resolution. In contrast, two phospholipid molecules, each with a hydrophilic head and two hydrophobic tails, could be ambiguously assigned in our structure (Figures 2B and S4F). We assume these molecules are one of the substrates, i.e., PS, PC or PE of ABCA7, which were extracted from the cell membrane. A closer look at the two binding sites of the hydrophilic head revealed mostly positively charged residues, including Lys567 at the cytoplasmic side, and Lys1406, Arg544 at the extracellular side, clearly better accommodating PS, which has a negatively charged head

Please cite this article in press as: Fang et al., Structural insights into human ABCA7-mediated lipid transport, Structure (2024), https://doi.org/10.1016/j.str.2024.12.015

CellPress

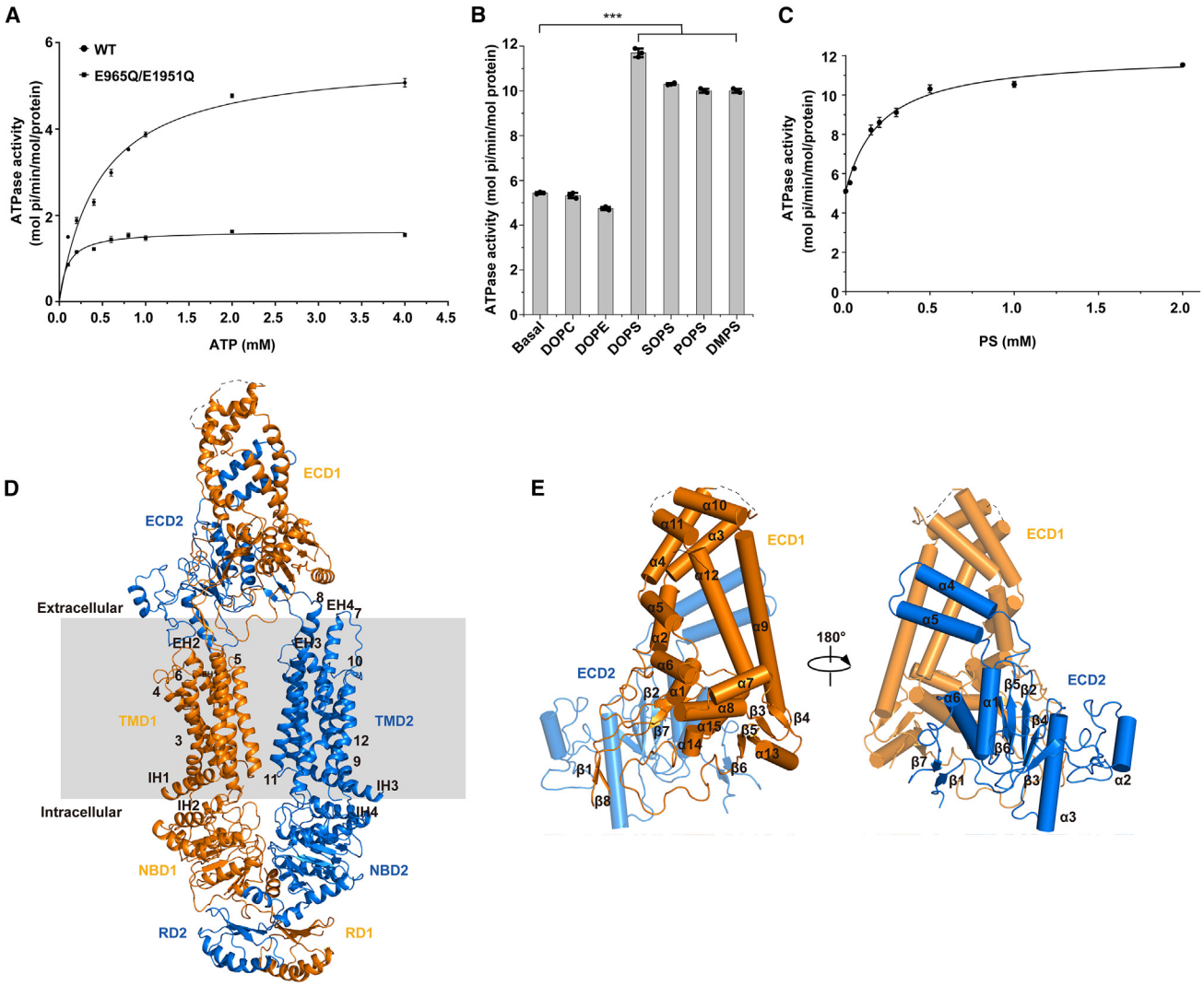

Figure 1. Substrate-stimulated ATPase activity assays and the overall structure of the apo-form ABCA7

(A) ATPase activities of wild-type ABCA7 (WT) and E965Q/E1951Q mutant in detergent. The data points are fitted with a Michaelis-Menten equation. All data points represent the means ± SD of three independent experiments (n = 3) at 37°C, and error bars represent standard deviation.

(B) ATPase activities of ABCA7 in detergent upon the addition of different phospholipids. DOPS, dioleoylphosphatidylserine; DOPC, dioleoylphosphatidylcholine; DOPE, dioleoylphosphatidylethanolamine; SOPS, 1-stearoyl-2-oleoyl-*sn*-glycero-3-phospho-L-serine; DPPS, 1,2-dipalmitoyl-*sn*-glycero-3-phospho-L-serine; DMPS, 1,2-dimyristoyl-*sn*-glycero-3-phospho-L-serine. Unpaired two-sided t test is used for the comparison of statistical significance. The p values of <0.05, 0.01, and 0.001 are indicated with *, **, and ***, compared to the wild type. All data points represent the means ± SD of three independent experiments (n = 3) at 37°C, and error bars represent standard deviation.

(C) The PS concentration-dependent ATPase activities of WT in detergent. The data points are fitted with a Michaelis-Menten equation. All data points represent the means ± SD of three independent experiments (n = 3) at 37°C, and error bars represent standard deviation.

(D) Cartoon representation of the apo-form ABCA7. The two-halves of ABCA7 are colored in orange for TMD1, ECD1, NBD1 and RD1 and marine for TMD2, ECD2, NBD2 and RD2, respectively. The 12 transmembrane helices (TMs) are sequentially numbered. The cellular membrane is indicated as the gray rectangle. ECD, extracellular domain; NBD, nucleotide-binding domain; TMD, transmembrane domain; RD, regulatory domain; IH, intracellular helix; EH, extracellular helix.

(E) Close-up view of the ECDs. The α-helices and β-sheet in ECD1 (left) and ECD2 (right) are sequentially numbered, respectively.

(Figure 2C). Moreover, our biochemical assays also indicated that PS could significantly stimulate the ATPase activity of ABCA7 (Figure 1B). Thus, we tentatively fitted two molecules of DOPS (indicated as PS for short hereafter) into the densities, respectively (Figures 2B and S4F). Notably, the purification procedure was the same as $ABCA7_{E965Q/E1951Q}$. Therefore, we assume that the energy of ATP hydrolysis is needed for substrate translocation cycle, thus the state of substrate binding can be easily captured by cryo-EM.

Structural comparison with the apo-form structure of ABCA7 yielded an overall root-mean-square deviation (RMSD) of 1.93 Å over 1443 Cα atoms, indicating a similar conformation (Figure S5A). However, TMD2 displays higher conformational variations, as the RMSD is 2.75 Å over 250 TMD2 Cα atoms while

Please cite this article in press as: Fang et al., Structural insights into human ABCA7-mediated lipid transport, Structure (2024), https://doi.org/10.1016/j.str.2024.12.015

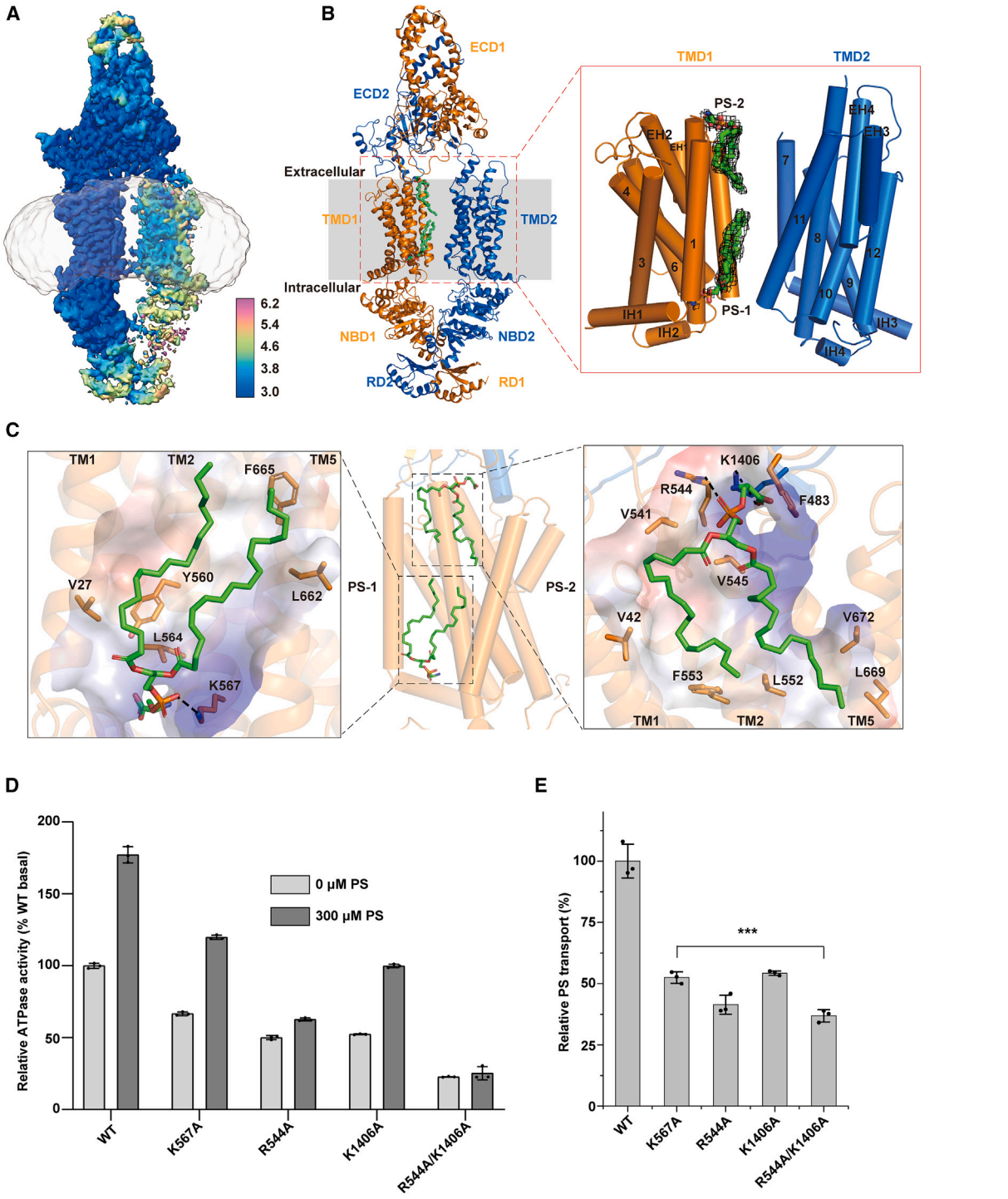

Figure 2. Overall structure of substrate-bound ABCA7 and the substrate-binding sites

(A) The local resolution map of substrate-bound ABCA7. The color code for resolutions, shown with the unit Å, is calculated using CryoSPARC. The cryo-EM map was colored by UCSF ChimeraX according to the local resolution estimated by cryoSPARC.

(B) Cartoon representation of the substrate-bound ABCA7 (left) and the close-up view of the TMDs (right). Two phosphatidylserine (PS) molecules are shown as green sticks. The cellular membrane is indicated as the gray rectangle. The 12 TMs, EHs, and IHs are sequentially numbered. Density maps of PS, shown as gray mesh. The density map of PS-1 is contoured at 3σ and the density map of PS-2 is contoured at 4σ. The density maps are carved at a distance of 2 Å.

(C) The binding sites of PS molecules. The interacting residues are shown as sticks and colored in orange from TMD1 or marine from ECD2. Hydrogen bonds are indicated by black dotted lines. Interacting residues of each PS molecule are shown by two zoom-in images, respectively. Two PS molecules are shown as green sticks. The electrostatic surface properties of the binding pocket are color-coded by electrostatic potential generated by PyMOL.

(legend continued on next page)

Please cite this article in press as: Fang et al., Structural insights into human ABCA7-mediated lipid transport, Structure (2024), https://doi.org/10.1016/j.str.2024.12.015

TMD1 can be perfectly superimposed (Figure S5B). In fact, TMD2 possesses a much lower local resolution in both of our structures (Figures 2A and S2C), as well as the previously reported ABCA7 structures.[34] Upon PS binding, most TMs in TMD2 rotate around the axis of TM8, leading to a more loosely packed TMD2 and a very flexible NBD2, which possesses a much lower resolution compared to that in the apo-form structure. For instance, TM12 moves ~6 Å, and the distal end of the coupling helix IH3 rotates of ~12° toward TMD1 (Figure S5B).

The two PS molecules stick on TMD1 in a "tail-to-tail" manner, along a groove formed by the helices TM1, TM2, and TM5 (Figure 2C). The PS molecule (termed PS-1 hereafter) at the inner leaflet of the cell membrane is fixed on TM5 via a salt bridge between its phosphate group and Lys567, with the hydrophilic head pointing toward the cytoplasm and the two hydrophobic acyl chain tails extending to the interface of the bilayer. Abundant hydrophobic residues, such as Leu564, Val27, Tyr560, Leu662, and Phe665 provide a hydrophobic environment to stabilize the acyl chains. In contrast, the other PS molecule at the outer leaflet (termed PS-2 hereafter) is fixed on TM2 and α3 helix of ECD2, via two salt bridges between the phosphate group and Arg554 of TM2, and the carboxyl group and Lys1406 of α3 helix, respectively. The two hydrophobic acyl chain tails of PS-2 also extend to the interface of the membrane bilayer, along the hydrophobic residues Phe483, Val541, Val42, Val545, Leu552, Phe553, Leu669, and Val672. Thus, the PS-1 and PS-2 adopt a "tail-to-tail" binding manner in the translocation cavity. Previous structures have revealed that the ECDs of ABCA1 possess an extra substrate binding site, suggesting that the substrate cholesterol should move from the TMDs to ECDs, and eventually be presented to ApoA-I to form the high-density lipoprotein.[39,40] Similarly, in the ECDs of the substrate-bound structure, we also found an extra electron microscopy density, which has an overall shape mimicking a phospholipid (Figure S5C). Despite this extra density is of rather low resolution, we proposed that ECDs of ABCA7 most likely also constitutes a part of the transport route that presents the substrate PS to the acceptor ApoE.

Using site-directed mutagenesis combined with PS-stimulated ATPase activity assays, we analyzed the key residues that form polar interactions with PS-1 and PS-2. The results indicated that all single mutants, including K567A, R544A, and K1406A, displayed a significant decrease in PS-simulated ATPase activity, compared to that of the wild type (Figure 2D). Moreover, double mutations of the two residues Arg544 and Lys1406 that cooperatively fix PS-2 to Ala showed the sharpest decrease of stimulate activity, almost comparable to the E965Q/E1951Q mutant that abolishes the ATPase activity (Figure 2D). In addition, the proteoliposome-based transport activity assays also revealed that all mutants showed significant decrease of transport activity, compared to the wild type (Figure 2E). Notably, the single mutant R544A and the double mutant R544A/K1406A displayed the lowest transport activity. These results indicated that the residues binding to PS-2 plays a rather more important role compared to those binding to PS-1.

Sequence alignment revealed that these positively charged residues that specifically binding to PS-1 and PS-2 are highly conserved among ABCA7 homologs (Figure S5D). Of note, Arg544, which is responsible for the recognition of the phosphate group of PS, is also conserved in human ABCA1. This is in accordance with that PS is reported to be one of the substrates of ABCA1.[33]

Superpositions between our present apo-form and PS-bound ABCA7 structures with the previously reported ABC7 structures,[34] respectively, revealed that the conformational changes are relatively subtle between apo-form and substrate-bound forms (Figure S5E). Of note, the RMSD of the superposition between our PS-bound structure and reported $ABCA7_{digitonin}$ are the smallest, which was described as the "intermediate open" state for the lipid flipping. Consistently, our PS-bound structure indeed illustrated an intermediate state of lipids in a "tail-to-tail" manner during flipping.

The PS transport activity of ABCA7 is enhanced in the presence of ApoE3

The human polymorphic *APOE* gene encodes one of the three isoforms of ApoE proteins (ApoE2, ApoE3, and ApoE4), which are different from each other in a single amino acid substitution at the N-terminal region.[41] ApoE3 is the most common (~77% frequency) isoform in populations, which were proposed to be a neutral isoform with respect to neurodegenerative disease risk.[42,43] In contrast, ~8% frequency that express ApoE2 (a R158C substitution) are of lower AD risk,[44] whereas ~15% that harbors ApoE4 (a C112R substitution) are statistically facing higher risk and early onset of AD.[45,46]

It has been proposed that ABCA7 could deliver phospholipids to ApoE.[24,25] However, direct biochemical evidences of whether ABCA7 could bind to ApoE still remain paucity. We recombinantly expressed ApoE2, ApoE3, and ApoE4 with a FLAG tag in HEK293 cells (Figure S5F), and performed pull-down assays. Here we found that all ApoE isoforms could be pulled-down by the His-tagged ABCA7 (Figures 3A and S5G). We also performed a pull-down assay with ApoE3 and another ABC transporter (ABCC3), which lacks ECD as control, and no ApoE3 could be detected in the elution samples. It indicated that there exist direct interactions between ABCA7 and ApoE. In the presence of ApoE, both the ATPase activity and PS-stimulated ATPase activity of ABCA7 are significantly increased (Figure 3B). Moreover, ABCA7 pre-incubated with excess ApoE3 showed a PS transport activity of ~4-folds compared to that of ABCA7 alone while ABCA7 pre-incubated with excess ApoE4 or ApoE2 showed a PS transport activity of ~2-folds (Figure 3C). The results showed

(D) Relative ATPase activities of wild-type ABCA7 (WT) and mutants in the presence of 2 mM ATP upon addition of PS in detergent. The ATPase activity was normalized relative to the basal ATPase activity of the WT. All data points represent the means ± SD of three independent experiments (n = 3) at 37°C, and error bars represent standard deviation.

(E) Relative PS transport activity assays of WT and mutants by protein reconstituted into porcine brain polar lipid (BPL) liposomes containing 0.6% (w/w) NBD-labeled PS. The activity of WT is set as 100%. All data points represent the means ± SD of three independent experiments (n = 3), and error bars represent standard deviation. Unpaired two-sided t test is used for the comparison of statistical significance. The p values of <0.05, 0.01 and 0.001 are indicated with *, **, and ***, compared to the WT.

Please cite this article in press as: Fang et al., Structural insights into human ABCA7-mediated lipid transport, Structure (2024), https://doi.org/10.1016/j.str.2024.12.015

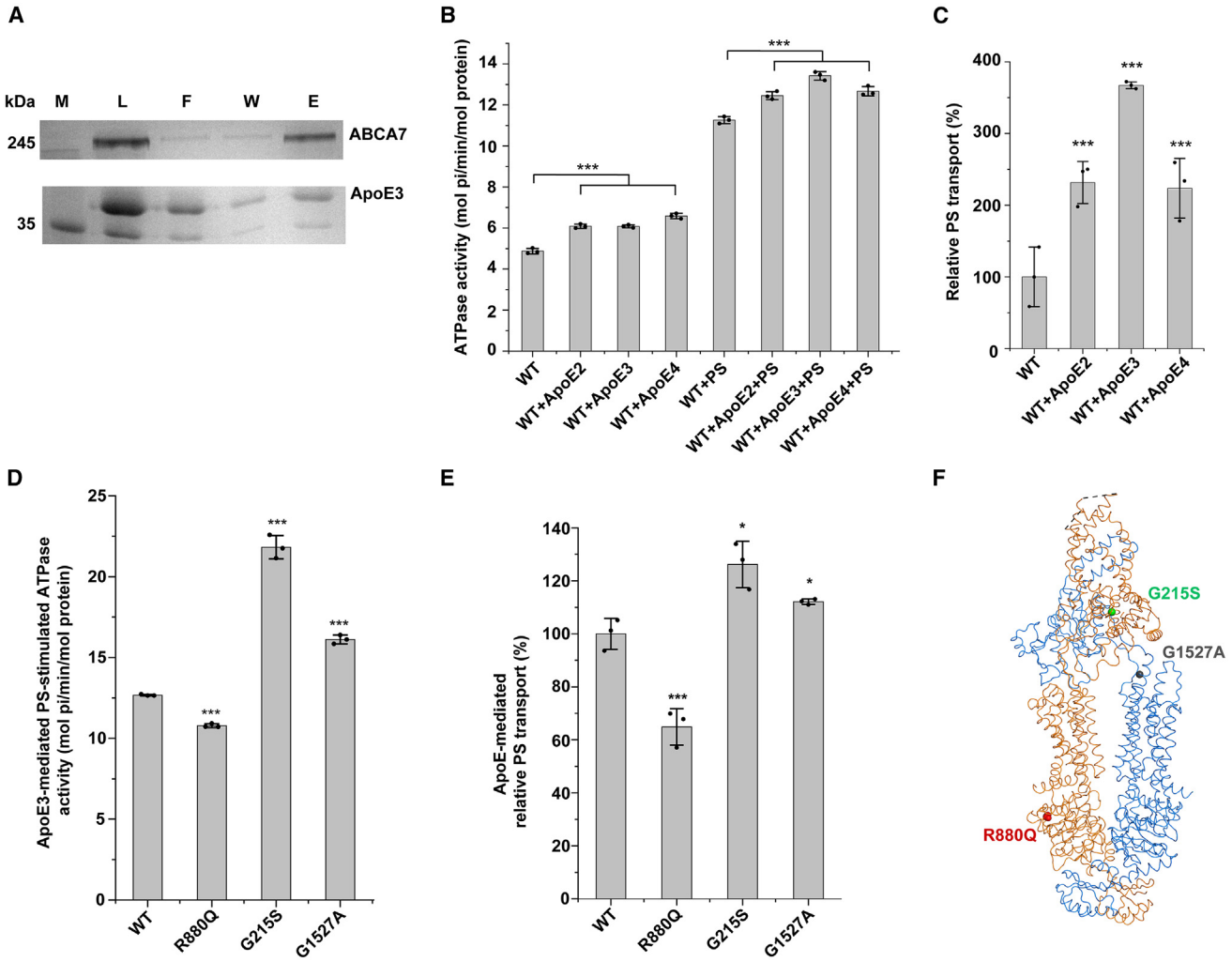

Figure 3. The biochemical assays of ABCA7 in the presence of ApoE

(A) SDS-PAGE gel of the samples of ABCA7-ApoE3 pull-down assay. M = molecular weight marker, L, ABCA7 + ApoE3 load. FT, flowthrough; W, final wash; E, eluate.

(B) ATPase activities of wild-type ABCA7 (WT) in the presence or absence of ApoE2, ApoE3, ApoE4 and DOPS. All data points represent the means ± SD of three independent experiments ($n = 3$), and error bars represent standard deviation. Unpaired two-sided t test is used for the comparison of statistical significance. The p values of <0.05, 0.01 and 0.001 are indicated with *, **, and ***, compared to WT.

(C) PS transport activity assays of WT in the presence of ApoE2, ApoE3 or ApoE4 by protein reconstituted into BPL liposomes containing 0.6% (w/w) NBD-PS. The activity of WT is set as 100%. The relative activity represents the PS transport activity of WT in the presence/absence of ApoE. All data points represent the means ± SD of three independent experiments ($n = 3$), and error bars represent standard deviation. Unpaired two-sided t test is used for the comparison of statistical significance. The p values of <0.05, 0.01 and 0.001 are indicated with *, **, and ***, compared to WT.

(D) ATPase activities of WT and AD-related variants of ABCA7 in the presence of 2 mM ATP upon addition of DOPS and ApoE3 in detergent. All data points represent the means ± SD of three independent experiments ($n = 3$), and error bars represent standard deviation. Unpaired two-sided t test is used for the comparison of statistical significance. The p values of <0.05, 0.01 and 0.001 are indicated with *, **, and ***, compared to WT.

(E) PS transport activity assays of WT and mutants that harboring a single mutation of residues related to AD by protein incubated with ApoE3 and then re-constituted into BPL liposomes containing 0.6% (w/w) NBD-PS. The activity of WT is set as 100%. The relative activity represents the PS transport activity of WT or its mutant. All data points represent the means ± SD of three independent experiments ($n = 3$), and error bars represent standard deviation. Unpaired two-sided t test is used for the comparison of statistical significance. The p values of <0.05, 0.01 and 0.001 are indicated with *, **, and ***, compared to WT.

(F) Mapping of three AD-related variants G1527A (gray sphere), R880Q (red sphere) and G215S (green sphere) on the structure of substrate-bound ABCA7.

that different ApoE isoforms could significantly increase the activities of ABCA7 with little discrepancies.

The clinic cases analysis indicated that the R880Q variant is correlated with the familial AD,[47] and the G215S and G1527A variants display lower risk of AD onset than WT ABCA7.[48–51] In consistence with the clinic reports, the R880Q mutant showed a significant lower PS-stimulated ATPase activity and PS transport activity, whereas the G215S and G1527A mutant displayed higher activities in both assays, compared to WT (Figures 3D and 3E). As shown in our structure, Arg880 in NBD1 points toward the interface between NBD1 and the corresponding coupling helix IH2 (Figures 3F and S6A). Thus, its mutation to a Glu residue

Please cite this article in press as: Fang et al., Structural insights into human ABCA7-mediated lipid transport, Structure (2024), https://doi.org/10.1016/j.str.2024.12.015

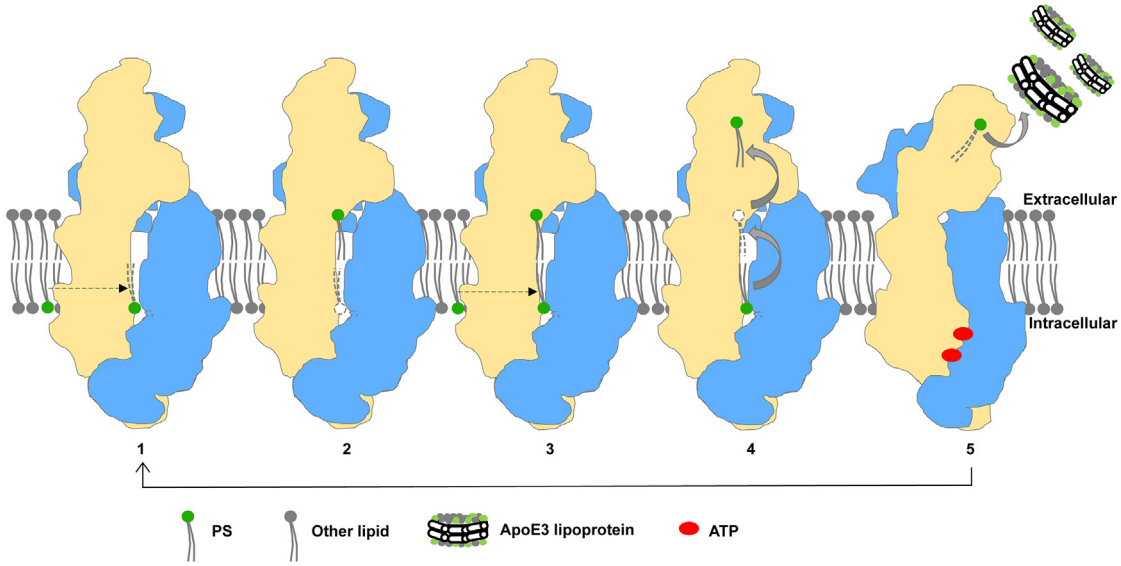

Figure 4. A proposed transport cycle of ABCA7

The transport cycle consists of five intermediate states: In the rest state, a PS molecule enters the translocation cavity via diffusion from the inner membrane leaflet (state 1). The stronger interactions between PS and its binding site at the outer membrane leaflet facilitate the flip of PS from the inner membrane leaflet (state 2), and the second PS molecule succeeds once the binding site at the inner membrane leaflet is vacant (state 3). A much narrowed translocation cavity occupied by two PS molecules further facilitates the exclusion of the first PS to the putative tunnel in ECDs (state 4). Upon ATP binding, ABCA7 shifts to a closed conformation due to the dimerization of NBDs. ECDs tilt and move toward TMD2, adopting a conformation favorable for presentation of PS to ApoE (state 5). Finally, ATP hydrolysis results in ABCA7 going back to the rest state for the next transport cycle.

should alter the interaction between NBD1 and IH2. In contrast, Gly215 in ECD1 is located at the exit of the extracellular tunnel (Figures 3F and S6B) that accommodates the third lipid. We hypothesized that a G215S mutation could increase the polarity of the exit, hence facilitating the translocation of PS molecules. On the other hand, Gly1527 in TMD2 is located at the interface between TMD2 and ECD, the mutation of G1527A might alter the interface conformation during PS transport (Figures 3F and S6C). Altogether, it suggested the ABCA7 activity may be somewhat correlated with the AD onset.

DISCUSSION

Many ABC transporters have been found to transport various kinds of lipids, cooperatively playing important roles in human lipid metabolism. Comparison of ABCA7 against other substrate-bound structures of these transporters, including ABCA3,[52] ABCA4,[38] and ABCB9,[53] offered some substrate-binding features (Figures S6D–S6G). Interestingly, the ABCA3 structure revealed only one substrate-binding pocket at the inner membrane leaflet which is similar to one of the two pockets of ABCA7. In ABCA4, a tentatively fitted PE molecule which was suggested to be a substrate of ABCA4,[33,54] was found to bind in a pocket at the inner membrane leaflet, with its polar head of phospholipids coordinated by Arg24 and Lys672, the importance of which were confirmed by ATPase activity assays.[38] Similarly, Lys21 and Arg280 in ABCA3 were also assumed to be responsible for binding to an unassigned lipid molecule.[52] In our ABCA7 structure, a counterpart residue Lys567 forms a hydrogen bond with the phosphate group of PS. Sequence alignment revealed that this positively charged residue is highly conserved (Figure S6H). In contrast, ABCB9 possesses a 1-palmitoyl-2-oleoyl-*sn*-glycero-3-phosphoglycerol (POPG) molecule binding to a pocket at the outer membrane leaflet,[53] which is similar to the other pocket in ABCA7. Similarly, another substrate molecule of N-retinylidene-PE was also found in a pocket in ABCA4 at the outer membrane leaflet. Altogether, it indicated that two sequential pockets are most likely necessary for the lipid export.

Therefore, in combination with all these structural information, we propose a phospholipid transport model from inner leaflet of the membrane to ApoE mediated by ABCA7 (Figure 4). At the rest state, ABCA7 adopts an OF conformation (state 1): a PS molecule (PS-1 in our case) from the inner membrane leaflet diffuses to the translocation cavity. The stronger interactions between PS and its binding site at the outer membrane leaflet might facilitate the flip of this PS from the inner membrane leaflet (state 2). Once the binding site at the inner membrane leaflet is vacant, the second PS molecule will succeed, resulting in two PS molecules simultaneously binding to TMD1, as captured in our substrate-bound structure (state 3). Notably, a much narrowed translocation cavity occupied by two PS molecules might further facilitate the exclusion of the first PS to the putative tunnel in ECDs (state 4). Upon ATP binding, ABCA7 shifts to a closed conformation due to the dimerization of NBDs (state 5). At this state, ECDs tilts and moves toward TMD2, adopting a conformation ready for the presentation of PS to ApoE, as previously illustrated.[34] Indeed, the ECDs of ATP-bound ABCA1 also harbor a cholesterol molecule that was proposed to be ready for presentation to ApoA-I.[39] Finally, ATP hydrolysis results in ABCA7 going back to the rest state for the next transport cycle.

ApoE is one of the commonly recognized risk factors of AD and has been suggested to be related to the production and

clearance of pathogenic protein Aβ, thus preventing AD.[43,55,56] Although both ABCA1 and ABCA7 are involved in the lipidation of ApoE, ABCA1 mainly delivers the cholesterol, whereas ABCA7 generally presents the phospholipids, to the apo-form ApoE, finally forming ApoE lipoproteins of different lipid content.[25] However, GWAS showed that ABCA1 is independent of AD onset, but ABCA7 shows a significant correlation with AD according to in-depth genetic studies.[57,58] It was reported that the *ABCA7* knock-out mice showed increased Aβ in the brain, in a manner independent of ApoE concentration.[59,60] Thus, we hypothesized the lipidation profile of ApoE particles mediated by ABCA7 might contribute to the variation (Figure S6I). In the presence of ABCA7, more PS will be presented to ApoE and form the so-called PS-rich ApoE particles, which is competent to other forms of lipids. Indeed, ApoE particles containing less lipids could specifically inhibit the γ-cleavage of APP,[55] whereas the particles containing less cholesterol are capable of extracting more cholesterol from the membrane of neurons that eventually leads to the normal α-cleavage of Amyloid-β precursor protein.[61] In addition, the higher abundancy of PS (PS-rich) in ApoE particles was reported to attribute to a lower binding affinity toward the ApoE receptor LRP1.[22] Moreover, a decreased binding affinity of ApoE toward the receptors on microglia was linked to a marked reduction in plaque-associated tau pathology, resulting in elimination of Aβ.[21] Altogether, the PS-rich ApoE particles, upon the transport of PS driven by ABCA7, will become more competent to other lipids or less recognized by the ApoE receptors, eventually contribute to decreased level of Aβ in brain.

In conclusion, these findings provide not only the two states in the PS transport cycle driven by ABCA7, but also the molecular evidence for the direct interplay between ABCA7 and ApoE, which is most likely correlated with the pathogenesis of AD.

RESOURCE AVAILABILITY

Lead contact

Further information and requests for resources and reagents should be directed to and will be fulfilled by the lead contact, Yuxing Chen (cyxing@ustc.edu.cn).

Materials availability

This study did not generate new unique reagents. All unique reagents generated in this study are available from the lead contact by request and with a completed materials transfer agreement.

Data and code availability

- Atomic coordinates and EM density maps of the human apo-form ABCA7 structure (PDB: 8Y1O; EMDB: EMD-38841) and ABCA7 structure complexed with PS (PDB: 8Y1P; EMDB: EMD-38842) in this paper have been deposited in the Protein DataBank and the Electron Microscopy DataBank, respectively. They are publicly available as of the date of publication. The accession codes are also listed in the key resources table.
- This paper does not report original code.
- Any additional information required to reanalyze the data reported in this paper is available from the lead contact upon request.

ACKNOWLEDGMENTS

We thank Dr. Yong-Xiang Gao at the Center for Integrative Imaging, University of Science and Technology of China during cryo-EM image acquisition. We thank Xu-Jing Li at the Center for Biological Imaging at the Institute of Biophysics (IBP), Chinese Academy of Sciences for technical support on cryo-EM data collection. We thank Professor Y.L, an investigator of SUSTech Institute for Biological Electron Microscopy. This work was supported by the Ministry of Science and Technology (China) of China (2020YFA0509302) and the Fundamental Research Funds for the Central Universities (YD9100002014 and WK9100000031).

AUTHOR CONTRIBUTIONS

S.-C.F. and Y.C. conceptualized this study. C.-Z.Z. and Y.C. supervised the project. S.-C.F. and W.-T.H. designed all the experiments. S.-C.F. performed cloning, expression, purification, EM sample preparation, screening, and analyses of human ABCA7. S.-C.F. and L.W. preformed cryo-EM data collection. S.-C.F., D.X., and Z.-P.C. performed ATPase activity assays. S.-C.F. and M.-T.C. performed lipid transport assays. S.-C.F., L.W., and J.W. performed structure determination and model refinement. S.-C.F., W.L., and Y.L. performed mass spectrometry assays. All authors contributed to data analysis. S.-C.F., W.-T.H., C.-Z.Z., and Y.C. wrote the manuscript.

DECLARATION OF INTERESTS

The authors declare no competing interests.

STAR★METHODS

Detailed methods are provided in the online version of this paper and include the following:

- KEY RESOURCES TABLE
- EXPERIMENTAL MODEL AND STUDY PARTICIPANT DETAILS
  - Cell culture
- METHOD DETAILS
  - Protein expression and purification
  - Pull-down assays
  - Lipid preparation
  - ATPase activity assays
  - Proteoliposome-based phosphatidylserine transport assay
  - Cryo-EM sample preparation and data collection
  - Cryo-EM data processing
  - Model building and refinement
- QUANTIFICATION AND STATISTICAL ANALYSIS

SUPPLEMENTAL INFORMATION

Supplemental information can be found online at https://doi.org/10.1016/j.str.2024.12.015.

Received: September 3, 2024
Revised: November 14, 2024
Accepted: December 19, 2024
Published: January 17, 2025

REFERENCES

1. Scheltens, P., De Strooper, B., Kivipelto, M., Holstege, H., Chételat, G., Teunissen, C.E., Cummings, J., and van der Flier, W.M. (2021). Alzheimer's disease. Lancet *397*, 1577–1590. https://doi.org/10.1016/s0140-6736(20)32205-4.
2. Zhang, T., Ma, S., Lv, J., Wang, X., Afewerky, H.K., Li, H., and Lu, Y. (2021). The emerging role of exosomes in Alzheimer's disease. Ageing Res. Rev. *68*, 101321. https://doi.org/10.1016/j.arr.2021.101321.
3. Scheltens, P., Blennow, K., Breteler, M.M.B., de Strooper, B., Frisoni, G.B., Salloway, S., and Van der Flier, W.M. (2016). Alzheimer's disease. Lancet *388*, 505–517. https://doi.org/10.1016/S0140-6736(15)01124-1.

4. Irwin, M.R., and Vitiello, M.V. (2019). Implications of sleep disturbance and inflammation for Alzheimer's disease dementia. Lancet Neurol. *18*, 296–306. https://doi.org/10.1016/s1474-4422(18)30450-2.

5. Moulton, P.V., and Yang, W. (2012). Air pollution, oxidative stress, and Alzheimer's disease. J. Environ. Public Health *2012*, 472751. https://doi.org/10.1155/2012/472751.

6. Cataldo, J.K., Prochaska, J.J., and Glantz, S.A. (2010). Cigarette smoking is a risk factor for Alzheimer's Disease: an analysis controlling for tobacco industry affiliation. J. Alzheimers Dis. *19*, 465–480. https://doi.org/10.3233/jad-2010-1240.

7. Hu, N., Yu, J.T., Tan, L., Wang, Y.L., Sun, L., and Tan, L. (2013). Nutrition and the risk of Alzheimer's disease. BioMed Res. Int. *2013*, 524820. https://doi.org/10.1155/2013/524820.

8. Sierksma, A., Escott-Price, V., and De Strooper, B. (2020). Translating genetic risk of Alzheimer's disease into mechanistic insight and drug targets. Science *370*, 61–66. https://doi.org/10.1126/science.abb8575.

9. Bagyinszky, E., Youn, Y.C., An, S.S.A., and Kim, S. (2014). The genetics of Alzheimer's disease. Clin. Interv. Aging *9*, 535–551. https://doi.org/10.2147/cia.S51571.

10. Kunkle, B.W., Grenier-Boley, B., Sims, R., Bis, J.C., Damotte, V., Naj, A.C., Boland, A., Vronskaya, M., van der Lee, S.J., Amlie-Wolf, A., et al. (2019). Genetic meta-analysis of diagnosed Alzheimer's disease identifies new risk loci and implicates Aβ, tau, immunity and lipid processing. Nat. Genet. *51*, 414–430. https://doi.org/10.1038/s41588-019-0358-2.

11. Lambert, J.C., Ibrahim-Verbaas, C.A., Harold, D., Naj, A.C., Sims, R., Bellenguez, C., DeStafano, A.L., Bis, J.C., Beecham, G.W., Grenier-Boley, B., et al. (2013). Meta-analysis of 74,046 individuals identifies 11 new susceptibility loci for Alzheimer's disease. Nat. Genet. *45*, 1452–1458. https://doi.org/10.1038/ng.2802.

12. Belloy, M.E., Napolioni, V., and Greicius, M.D. (2019). A Quarter Century of APOE and Alzheimer's Disease: Progress to Date and the Path Forward. Neuron *101*, 820–838. https://doi.org/10.1016/j.neuron.2019.01.056.

13. Long, J.M., and Holtzman, D.M. (2019). Alzheimer Disease: An Update on Pathobiology and Treatment Strategies. Cell *179*, 312–339. https://doi.org/10.1016/j.cell.2019.09.001.

14. Montagne, A., Nation, D.A., Sagare, A.P., Barisano, G., Sweeney, M.D., Chakhoyan, A., Pachicano, M., Joe, E., Nelson, A.R., D'Orazio, L.M., et al. (2020). APOE4 leads to blood–brain barrier dysfunction predicting cognitive decline. Nature *581*, 71–76. https://doi.org/10.1038/s41586-020-2247-3.

15. Yang, L.G., March, Z.M., Stephenson, R.A., and Narayan, P.S. (2023). Apolipoprotein E in lipid metabolism and neurodegenerative disease. Trends Endocrinol. Metabol. *34*, 430–445. https://doi.org/10.1016/j.tem.2023.05.002.

16. Mahley, R.W., Weisgraber, K.H., and Huang, Y. (2009). Apolipoprotein E: structure determines function, from atherosclerosis to Alzheimer's disease to AIDS. J. Lipid Res. *50*, S183–S188. https://doi.org/10.1194/jlr.R800069-JLR200.

17. Chen, Y., Strickland, M.R., Soranno, A., and Holtzman, D.M. (2021). Apolipoprotein E: Structural Insights and Links to Alzheimer Disease Pathogenesis. Neuron *109*, 205–221. https://doi.org/10.1016/j.neuron.2020.10.008.

18. Mahley, R.W. (2016). Central Nervous System Lipoproteins: ApoE and Regulation of Cholesterol Metabolism. Arterioscler. Thromb. Vasc. Biol. *36*, 1305–1315. https://doi.org/10.1161/atvbaha.116.307023.

19. Kowal, R.C., Herz, J., Goldstein, J.L., Esser, V., and Brown, M.S. (1989). Low density lipoprotein receptor-related protein mediates uptake of cholesteryl esters derived from apoprotein E-enriched lipoproteins. Proc. Natl. Acad. Sci. USA *86*, 5810–5814. https://doi.org/10.1073/pnas.86.15.5810.

20. Hui, D.Y., Innerarity, T.L., and Mahley, R.W. (1984). Defective hepatic lipoprotein receptor binding of beta-very low density lipoproteins from type III hyperlipoproteinemic patients. Importance of apolipoprotein E. J. Biol. Chem. *259*, 860–869.

21. Chen, Y., Song, S., Parhizkar, S., Lord, J., Zhu, Y., Strickland, M.R., Wang, C., Park, J., Tabor, G.T., Jiang, H., et al. (2024). APOE3ch alters microglial response and suppresses Aβ-induced tau seeding and spread. Cell *187*, 428–445.e20. https://doi.org/10.1016/j.cell.2023.11.029.

22. Yamamoto, T., and Ryan, R.O. (2007). Anionic phospholipids inhibit apolipoprotein E--low-density lipoprotein receptor interactions. Biochem. Biophys. Res. Commun. *354*, 820–824. https://doi.org/10.1016/j.bbrc.2007.01.066.

23. Krimbou, L., Denis, M., Haidar, B., Carrier, M., Marcil, M., and Genest, J., Jr. (2004). Molecular interactions between apoE and ABCA1: impact on apoE lipidation. J. Lipid Res. *45*, 839–848. https://doi.org/10.1194/jlr.M300418-JLR200.

24. Wang, N., Lan, D., Gerbod-Giannone, M., Linsel-Nitschke, P., Jehle, A.W., Chen, W., Martinez, L.O., and Tall, A.R. (2003). ATP-binding cassette transporter A7 (ABCA7) binds apolipoprotein A-I and mediates cellular phospholipid but not cholesterol efflux. J. Biol. Chem. *278*, 42906–42912. https://doi.org/10.1074/jbc.M307831200.

25. Picataggi, A., Rodrigues, A., Cromley, D.A., Wang, H., Wiener, J.P., Garliyev, V., Billheimer, J.T., Grabiner, B.C., Hurt, J.A., Chen, A.C., et al. (2022). Specificity of ABCA7-mediated cell lipid efflux. Biochim. Biophys. Acta Mol. Cell Biol. Lipids *1867*, 159157. https://doi.org/10.1016/j.bbalip.2022.159157.

26. Bellenguez, C., Küçükali, F., Jansen, I.E., Kleineidam, L., Moreno-Grau, S., Amin, N., Naj, A.C., Campos-Martin, R., Grenier-Boley, B., Andrade, V., et al. (2022). New insights into the genetic etiology of Alzheimer's disease and related dementias. Nat. Genet. *54*, 412–436. https://doi.org/10.1038/s41588-022-01024-z.

27. De Roeck, A., Van den Bossche, T., van der Zee, J., Verheijen, J., De Coster, W., Van Dongen, J., Dillen, L., Baradaran-Heravi, Y., Heeman, B., Sanchez-Valle, R., et al. (2017). Deleterious ABCA7 mutations and transcript rescue mechanisms in early onset Alzheimer's disease. Acta Neuropathol. *134*, 475–487. https://doi.org/10.1007/s00401-017-1714-x.

28. Qian, X.H., Chen, S.Y., Liu, X.L., and Tang, H.D. (2023). ABCA7-Associated Clinical Features and Molecular Mechanisms in Alzheimer's Disease. Mol. Neurobiol. *60*, 5548–5556. https://doi.org/10.1007/s12035-023-03414-8.

29. De Roeck, A., Van Broeckhoven, C., and Sleegers, K. (2019). The role of ABCA7 in Alzheimer's disease: evidence from genomics, transcriptomics and methylomics. Acta Neuropathol. *138*, 201–220. https://doi.org/10.1007/s00401-019-01994-1.

30. Martens, Y.A., Zhao, N., Liu, C.C., Kanekiyo, T., Yang, A.J., Goate, A.M., Holtzman, D.M., and Bu, G. (2022). ApoE Cascade Hypothesis in the pathogenesis of Alzheimer's disease and related dementias. Neuron *110*, 1304–1317. https://doi.org/10.1016/j.neuron.2022.03.004.

31. Aikawa, T., Holm, M.L., and Kanekiyo, T. (2018). ABCA7 and Pathogenic Pathways of Alzheimer's Disease. Brain Sci. *8*, 27. https://doi.org/10.3390/brainsci8020027.

32. Dib, S., Pahnke, J., and Gosselet, F. (2021). Role of ABCA7 in Human Health and in Alzheimer's Disease. Int. J. Mol. Sci. *22*, 4603. https://doi.org/10.3390/ijms22094603.

33. Quazi, F., and Molday, R.S. (2013). Differential phospholipid substrates and directional transport by ATP-binding cassette proteins ABCA1, ABCA7, and ABCA4 and disease-causing mutants. J. Biol. Chem. *288*, 34414–34426. https://doi.org/10.1074/jbc.M113.508812.

34. Le, L.T.M., Thompson, J.R., Dehghani-Ghahnaviyeh, S., Pant, S., Dang, P.X., French, J.B., Kanikeyo, T., Tajkhorshid, E., and Alam, A. (2023). Cryo-EM structures of human ABCA7 provide insights into its phospholipid translocation mechanisms. EMBO J. *42*, e111065. https://doi.org/10.15252/embj.2022111065.

35. Tomioka, M., Toda, Y., Mañucat, N.B., Akatsu, H., Fukumoto, M., Kono, N., Arai, H., Kioka, N., and Ueda, K. (2017). Lysophosphatidylcholine export by human ABCA7. Biochim. Biophys. Acta Mol. Cell Biol. Lipids *1862*, 658–665. https://doi.org/10.1016/j.bbalip.2017.03.012.

36. Thomas, C., and Tampé, R. (2020). Structural and Mechanistic Principles of ABC Transporters. Annu. Rev. Biochem. *89*, 605–636. https://doi.org/10.1146/annurev-biochem-011520-105201.

37. Qian, H., Zhao, X., Cao, P., Lei, J., Yan, N., and Gong, X. (2017). Structure of the Human Lipid Exporter ABCA1. Cell *169*, 1228–1239.e10. https://doi.org/10.1016/j.cell.2017.05.020.

38. Xie, T., Zhang, Z., Fang, Q., Du, B., and Gong, X. (2021). Structural basis of substrate recognition and translocation by human ABCA4. Nat. Commun. *12*, 3853. https://doi.org/10.1038/s41467-021-24194-6.

39. Sun, Y., and Li, X. (2022). Cholesterol efflux mechanism revealed by structural analysis of human ABCA1 conformational states. Nat. Cardiovasc. Res. *1*, 238–245. https://doi.org/10.1038/s44161-022-00022-y.

40. Segrest, J.P., Tang, C., Song, H.D., Jones, M.K., Davidson, W.S., Aller, S.G., and Heinecke, J.W. (2022). ABCA1 is an extracellular phospholipid translocase. Nat. Commun. *13*, 4812. https://doi.org/10.1038/s41467-022-32437-3.

41. Kanekiyo, T., Xu, H., and Bu, G. (2014). ApoE and Aβ in Alzheimer's disease: accidental encounters or partners? Neuron *81*, 740–754. https://doi.org/10.1016/j.neuron.2014.01.045.

42. Huang, Y., and Mahley, R.W. (2014). Apolipoprotein E: structure and function in lipid metabolism, neurobiology, and Alzheimer's diseases. Neurobiol. Dis. *72*, 3–12. https://doi.org/10.1016/j.nbd.2014.08.025.

43. Liu, C.C., Liu, C.C., Kanekiyo, T., Xu, H., and Bu, G. (2013). Apolipoprotein E and Alzheimer disease: risk, mechanisms and therapy. Nat. Rev. Neurol. *9*, 106–118. https://doi.org/10.1038/nrneurol.2012.263.

44. Li, Z., Shue, F., Zhao, N., Shinohara, M., and Bu, G. (2020). APOE2: protective mechanism and therapeutic implications for Alzheimer's disease. Mol. Neurodegener. *15*, 63. https://doi.org/10.1186/s13024-020-00413-4.

45. Corder, E.H., Saunders, A.M., Strittmatter, W.J., Schmechel, D.E., Gaskell, P.C., Small, G.W., Roses, A.D., Haines, J.L., and Pericak-Vance, M.A. (1993). Gene dose of apolipoprotein E type 4 allele and the risk of Alzheimer's disease in late onset families. Science *261*, 921–923. https://doi.org/10.1126/science.8346443.

46. Rebeck, G.W., Reiter, J.S., Strickland, D.K., and Hyman, B.T. (1993). Apolipoprotein E in sporadic Alzheimer's disease: allelic variation and receptor interactions. Neuron *11*, 575–580. https://doi.org/10.1016/0896-6273(93)90070-8.

47. May, P., Pichler, S., Hartl, D., Bobbili, D.R., Mayhaus, M., Spaniol, C., Kurz, A., Balling, R., Schneider, J.G., and Riemenschneider, M. (2018). Rare ABCA7 variants in 2 German families with Alzheimer disease. Neurol. Genet. *4*, e224. https://doi.org/10.1212/nxg.0000000000000224.

48. Sassi, C., Nalls, M.A., Ridge, P.G., Gibbs, J.R., Ding, J., Lupton, M.K., Troakes, C., Lunnon, K., Al-Sarraj, S., Brown, K.S., et al. (2016). ABCA7 p.G215S as potential protective factor for Alzheimer's disease. Neurobiol. Aging *46*, 235.e1–235.e9. https://doi.org/10.1016/j.neurobiolaging.2016.04.004.

49. Hollingworth, P., Harold, D., Sims, R., Gerrish, A., Lambert, J.C., Carrasquillo, M.M., Abraham, R., Hamshere, M.L., Pahwa, J.S., Moskvina, V., et al. (2011). Common variants at ABCA7, MS4A6A/MS4A4E, EPHA1, CD33 and CD2AP are associated with Alzheimer's disease. Nat. Genet. *43*, 429–435. https://doi.org/10.1038/ng.803.

50. Dong, L., Mao, C., Liu, C., Li, J., Huang, X., Wang, J., Lei, D., Chu, S., Sha, L., Xu, Q., et al. (2022). Association Between Common Variants of APOE, ABCA7, A2M, BACE1, and Cerebrospinal Fluid Biomarkers in Alzheimer's Disease: Data from the PUMCH Dementia Cohort. J. Alzheimers Dis. *85*, 1511–1518. https://doi.org/10.3233/jad-215067.

51. Fehér, Á., Juhász, A., Pákáski, M., Janka, Z., and Kálmán, J. (2019). Association study of the ABCA7 rs3752246 polymorphism in Alzheimer's disease. Psychiatr. Res. *279*, 376–377. https://doi.org/10.1016/j.psychres.2019.01.081.

52. Xie, T., Zhang, Z., Yue, J., Fang, Q., and Gong, X. (2022). Cryo-EM structures of the human surfactant lipid transporter ABCA3. Sci. Adv. *8*, eabn3727. https://doi.org/10.1126/sciadv.abn3727.

53. Park, J.G., Kim, S., Jang, E., Choi, S.H., Han, H., Ju, S., Kim, J.W., Min, D.S., and Jin, M.S. (2022). The lysosomal transporter TAPL has a dual role as peptide translocator and phosphatidylserine floppase. Nat. Commun. *13*, 5851. https://doi.org/10.1038/s41467-022-33593-2.

54. Quazi, F., Lenevich, S., and Molday, R.S. (2012). ABCA4 is an N-retinylidene-phosphatidylethanolamine and phosphatidylethanolamine importer. Nat. Commun. *3*, 925. https://doi.org/10.1038/ncomms1927.

55. Hou, X., Zhang, X., Zou, H., Guan, M., Fu, C., Wang, W., Zhang, Z.R., Geng, Y., and Chen, Y. (2023). Differential and substrate-specific inhibition of γ-secretase by the C-terminal region of ApoE2, ApoE3, and ApoE4. Neuron *111*, 1898–1913.e5. https://doi.org/10.1016/j.neuron.2023.03.024.

56. Bales, K.R., Verina, T., Cummins, D.J., Du, Y., Dodel, R.C., Saura, J., Fishman, C.E., DeLong, C.A., Piccardo, P., Petegnief, V., et al. (1999). Apolipoprotein E is essential for amyloid deposition in the APP(V717F) transgenic mouse model of Alzheimer's disease. Proc. Natl. Acad. Sci. USA *96*, 15233–15238. https://doi.org/10.1073/pnas.96.26.15233.

57. Kunkle, B.W., Grenier-Boley, B., Sims, R., Bis, J.C., Damotte, V., Naj, A.C., Boland, A., Vronskaya, M., van der Lee, S.J., Amlie-Wolf, A., et al. (2019). Genetic meta-analysis of diagnosed Alzheimer's disease identifies new risk loci and implicates Aβ, tau, immunity and lipid processing. Nat. Genet. *51*, 414–430. https://doi.org/10.1038/s41588-019-0358-2.

58. Schwartzentruber, J., Cooper, S., Liu, J.Z., Barrio-Hernandez, I., Bello, E., Kumasaka, N., Young, A.M.H., Franklin, R.J.M., Johnson, T., Estrada, K., et al. (2021). Genome-wide meta-analysis, fine-mapping and integrative prioritization implicate new Alzheimer's disease risk genes. Nat. Genet. *53*, 392–402. https://doi.org/10.1038/s41588-020-00776-w.

59. Satoh, K., Abe-Dohmae, S., Yokoyama, S., St George-Hyslop, P., and Fraser, P.E. (2015). ATP-binding cassette transporter A7 (ABCA7) loss of function alters Alzheimer amyloid processing. J. Biol. Chem. *290*, 24152–24165. https://doi.org/10.1074/jbc.M115.655076.

60. Kim, W.S., Li, H., Ruberu, K., Chan, S., Elliott, D.A., Low, J.K., Cheng, D., Karl, T., and Garner, B. (2013). Deletion of Abca7 increases cerebral amyloid-beta accumulation in the J20 mouse model of Alzheimer's disease. J. Neurosci. *33*, 4387–4394. https://doi.org/10.1523/JNEUROSCI.4165-12.2013.

61. Wang, H., Kulas, J.A., Wang, C., Holtzman, D.M., Ferris, H.A., and Hansen, S.B. (2021). Regulation of beta-amyloid production in neurons by astrocyte-derived cholesterol. Proc. Natl. Acad. Sci. USA *118*, e2102191118. https://doi.org/10.1073/pnas.2102191118.

62. Mastronarde, D.N. (2005). Automated electron microscope tomography using robust prediction of specimen movements. J. Struct. Biol. *152*, 36–51. https://doi.org/10.1016/j.jsb.2005.07.007.

63. Zheng, S.Q., Palovcak, E., Armache, J.P., Verba, K.A., Cheng, Y., and Agard, D.A. (2017). MotionCor2: anisotropic correction of beam-induced motion for improved cryo-electron microscopy. Nat. Methods *14*, 331–332. https://doi.org/10.1038/nmeth.4193.

64. Rohou, A., and Grigorieff, N. (2015). CTFFIND4: Fast and accurate defocus estimation from electron micrographs. J. Struct. Biol. *192*, 216–221. https://doi.org/10.1016/j.jsb.2015.08.008.

65. Punjani, A., Rubinstein, J.L., Fleet, D.J., and Brubaker, M.A. (2017). cryoSPARC: algorithms for rapid unsupervised cryo-EM structure determination. Nat. Methods *14*, 290–296. https://doi.org/10.1038/nmeth.4169.

66. Pettersen, E.F., Goddard, T.D., Huang, C.C., Couch, G.S., Greenblatt, D.M., Meng, E.C., and Ferrin, T.E. (2004). UCSF Chimera–a visualization system for exploratory research and analysis. J. Comput. Chem. *25*, 1605–1612. https://doi.org/10.1002/jcc.20084.

67. Emsley, P., Lohkamp, B., Scott, W.G., and Cowtan, K. (2010). Features and development of Coot. Acta Crystallogr. D Biol. Crystallogr. *66*, 486–501. https://doi.org/10.1107/s0907444910007493.

68. Adams, P.D., Afonine, P.V., Bunkóczi, G., Chen, V.B., Davis, I.W., Echols, N., Headd, J.J., Hung, L.W., Kapral, G.J., Grosse-Kunstleve, R.W., et al. (2010). PHENIX: a comprehensive Python-based system for macromolecular structure solution. Acta Crystallogr. D Biol. Crystallogr. *66*, 213–221. https://doi.org/10.1107/s0907444909052925.

69. Schneider, C.A., Rasband, W.S., and Eliceiri, K.W. (2012). NIH Image to ImageJ: 25 years of image analysis. Nat. Methods *9*, 671–675. https://doi.org/10.1038/nmeth.2089.

70. Emsley, P., and Cowtan, K. (2004). Coot: model-building tools for molecular graphics. Acta Crystallogr. D Biol. Crystallogr. *60*, 2126–2132. https://doi.org/10.1107/s0907444904019158.

71. Waterhouse, A., Bertoni, M., Bienert, S., Studer, G., Tauriello, G., Gumienny, R., Heer, F.T., de Beer, T.A.P., Rempfer, C., Bordoli, L., et al. (2018). SWISS-MODEL: homology modelling of protein structures and complexes. Nucleic Acids Res. *46*. W296-w303. https://doi.org/10.1093/nar/gky427.

Please cite this article in press as: Fang et al., Structural insights into human ABCA7-mediated lipid transport, Structure (2024), https://doi.org/10.1016/j.str.2024.12.015

STAR★METHODS

KEY RESOURCES TABLE

REAGENT or RESOURCE	SOURCE	IDENTIFIER
Bacterial and virus strains		
TOP10 Chemically Competent Cells	Tsingke Biological Technology	Cat#TSC-C12
Chemicals, peptides, and recombinant proteins		
SMM 293-TII Expression Medium	Sino Biological	Cat#M293TII
Polyethylenimine, Linear, MW 25000	Polysciences	Cat#23966-1; CAS: 9002-98-6, 26913-06-4
Sodium butyrate	Aladdin	Cat#S102956; CAS:156-54-7
EDTA free Protease Inhibitor Cocktail	TargetMol	Cat#C0001
Cholesteryl hemisuccinate tris salt (CHS)	Anatrace	Cat#CH210
n-Dodecyl-β-D-Maltopyranoside (DDM)	Anatrace	Cat#D310A
18:1 PS (DOPS)	Avanti	Cat#840035P
18:1 PC (DOPC)	Avanti	Cat#850375P
18:1 PE (DOPE)	Avanti	Cat#850725P
Glycodiosgenin (GDN)	Anatrace	Cat#GDN101
Brain Polar Extract Phospholipid Profile (BPL)	Avanti	Cat#141101P
18:0-18:1 PS (POPS)	Avanti	Cat#840039P
16:0 PS	Avanti	Cat#840037P
14:0 PS	Avanti	Cat#840033P
18:1-06:0 NBD PS (NBD-PS)	Avanti	Cat#810194P
18:1-06:0 NBD PC (NBD-PC)	Avanti	Cat#810132P
18:1-06:0 NBD PE (NBD-PE)	Avanti	Cat#810155P
ATP	Sigma Aldrich	Cat#A2383
Bio-Beads SM-2 Resin	Bio-Rad	Cat#1523920
Triton X-100	Thermo Scientific	Cat#85111
Critical commercial assays		
ATPase Activity Kit (Colorimetric)	Innova Biosciences	Cat#601-0120
Deposited data		
Coordinates of human ABCA7 in the apo state	This paper	PDB: 8Y1O
Cryo-EM map of human ABCA7 in the apo state	This paper	EMD-38841
Coordinates of human ABCA7 in the lipid-bound state	This paper	PDB: 8Y1P
Cryo-EM map of human ABCA7 in the lipid-bound state	This paper	EMD-38842
Experimental models: Cell lines		
HEK 293F	Invitrogen	Cat#R79007
Oligonucleotides		
Oligonucleotides used in this study are listed in Table S3	This paper	N/A
Recombinant DNA		
Codon-optimized human *ABCA7* (isoform 1)	This paper	N/A
Codon-optimized human *APOE*	This paper	N/A
Codon-optimized human *ABCC3*	This paper	N/A
Modified pcDNA3.1 vector suitable for expression in mammalian cells	This paper	N/A
pCAG-ABCA7(WT)-FLAG	This paper	N/A
pCAG-ABCA7(E965Q/E1951Q)-FLAG	This paper	N/A
pCAG-ABCA7(K567A)-FLAG	This paper	N/A
pCAG-ABCA7(R544A)-FLAG	This paper	N/A

(*Continued on next page*)

Please cite this article in press as: Fang et al., Structural insights into human ABCA7-mediated lipid transport, Structure (2024), https://doi.org/10.1016/j.str.2024.12.015

Continued

REAGENT or RESOURCE	SOURCE	IDENTIFIER
pCAG-ABCA7(K1406A)-FLAG	This paper	N/A
pCAG-ABCA7(G215S)-FLAG	This paper	N/A
pCAG-ABCA7(R880Q)-FLAG	This paper	N/A
pCAG-ABCA7(R544A/K1406A)-FLAG	This paper	N/A
pCAG-ABCA7(G1527A)-FLAG	This paper	N/A
Software and algorithms		
SerialEM	Mastronarde (2005)[62]	https://bio3d.colorado.edu/SerialEM/
MotionCor2	Zheng et al. (2017)[63]	https://msg.ucsf.edu/software
CTFFIND4	Rohou and Grigorieff (2015)[64]	http://grigoriefflab.janelia.org/ctffind4
cryoSPARC	Punjani et al. (2017)[65]	https://cryosparc.com
UCSF Chimera	Pettersen et al. (2004)[66]	https://www.cgl.ucsf.edu/chimera
COOT	Emsley et al. (2010)[67]	https://www2.mrclmb.cam.ac.uk/personal/pemsley/coot/
PHENIX	Adams et al. (2010)[68]	https://phenix-online.org
PyMOL	PyMOL[69]	http://www.pymol.org
OriginPro	N/A	https://www.originlab.com/Origin
Graphpad Prism	N/A	https://www.graphpad.com
Other		
Gold Mix (green)	Tsingke Biological Technology	Cat#TSE102
Quantifoil R1.2/1.3 300 mesh Au holey carbon grids	Quantifoil	Cat#X-101-Au300
Superdex® 200 Increase 10/300 GL	GE Healthcare	Cat#GE28-9909-44
BeyoGel™ Plus Precast PAGE Gel (8 to 15%) for Tris-Gly System	Beyotime	Cat#P0472S
Unstained Protein MW Marker	Thermo Scientific	Cat#26610
ColorMixed Protein Marker	Beijing Solarbio Science & Technology	Cat#PR1920

EXPERIMENTAL MODEL AND STUDY PARTICIPANT DETAILS

Cell culture

HEK 293F cells used for protein expression were obtained from Invitrogen (#R79007, China) and cultured in SMM 293T-II medium (Sino Biological Inc.) at 37°C, supplemented with 5% CO2. The cell transfection was manipulated when cell density reached ~2.5 × 106 cells per mL.

METHOD DETAILS

Protein expression and purification

The full-length human *ABCA7* gene (Uniprot ID: Q8IZY2-1, isoform1) was synthesized by General Biosystems Company after codon optimization by eukaryotic expression system, and then subcloned into a pCAG vector with a C-terminal Flag-tag (DYKDDDDK) using a ClonExpress II One Step Cloning Kit (C113-02, Vazyme Biotech co., Ltd.). All single mutants of ABCA7 were constructed by a standard two-step PCR strategy and verified by DNA sequencing (Sangon Biotech Shanghai Co., Ltd.). The primers were synthesized by Sangon Biotech.

For protein expression, HEK293 cells (R79007, Invitrogen) were cultured in SMM 293T-II medium (Sino Biological Inc.) at 37°C with 5% CO_2 in an incubator shaken at 130 rpm. Cells were transfected when the density reached ~2.5 ×10^6 cells per milliliter by adding ~1.5 mg recombinant plasmids premixed with 4 mg linear polyethylenimines (40816, Yeasen Biotechnology) in 45 mL fresh medium for 15 min. After 15 min static incubation, the transfected cells were grown at 37°C for 48 hr before harvesting. The cell pellets were resuspended in a lysis buffer containing 50 mM Tris-HCl pH 7.5, 150 mM NaCl, 20% glycerol (w/v) and protease inhibitor cocktail (C0001, TargetMol) after centrifugation at 5,000 rpm for 6 min. Then the suspension was frozen in liquid nitrogen and stored at -80°C for further experiments.

For protein purification, the thawed suspension was incubated in the lysis buffer with additional 1% (w/v) n-Dodecyl-β-D-maltoside (DDM, Anatrace), 0.2% (w/v) cholesteryl hemisuccinate (CHS, Anatrace) at 4°C for 2 hr with gentle rotation to solubilize membrane and extract protein. Insoluble material was removed by ultracentrifugation at 45,000 rpm for 45 min (Beckman, Type 70 Ti) at 4°C. The

Please cite this article in press as: Fang et al., Structural insights into human ABCA7-mediated lipid transport, Structure (2024), https://doi.org/10.1016/j.str.2024.12.015

supernatant was incubated in a decolorization shaker with the anti-FLAG M2 affinity gel (Sigma-Aldrich) on ice for 1 hr. The resin was then loaded onto the column and washed five times, each time with 5 mL of wash buffer containing 50 mM Tris-HCl pH 7.5, 150 mM NaCl, 10% (w/v) glycerol and 0.02% (w/v) glycodiosgenin (GDN, Anatrace). Protein was eluted in batches to 6 mL after 20 min incubation with elution buffer containing 50 mM Tris-HCl pH 7.5, 150 mM NaCl, 5% (w/v) glycerol, 0.02% (w/v) GDN plus 200 μg/mL FLAG peptide. The eluate was then collected and concentrated using a 100-kDa MWCO Amicon Ultra centrifugal filter (Millipore) before being applied to size-exclusion chromatography by a Superose 6 Increase 10/300 gel filtration column (Cytiva) equilibrated in 50 mM Tris pH 7.5, 150 mM NaCl, and 0.02% (w/v) GDN. The peak fractions were collected and concentrated. The purified samples were analyzed by SDS-gel electrophoresis and then frozen by liquid nitrogen, and stored at -80°C before use. All steps were performed either in cold storage or on ice. The purification and expression of ABCC3 and mutants of ABCA7 were same to that of wild type ABCA7.

The purification and expression of ApoE3 was similar to that of ABCA7. The difference was that the method of pressure disruption was used when solubilizing the membrane for ApoE3 protein. Specifically, cells expressing ApoE3 protein were disrupted using a pressure of 600 MPa. After centrifugation at 12,000 rpm for 30 min at 4°C, the supernatant was incubated with anti-FLAG M2 affinity gel on ice for 1 hr. Subsequent steps were consistent with the purification of ABCA7 except that no detergents were added. The eluate was then collected and concentrated using a 30-kDa MWCO Amicon Ultra centrifugal filter (Millipore) before being applied to size-exclusion chromatography by a Superdex® 200 Increase 10/300 gel filtration column (Cytiva) equilibrated in 50 mM Tris pH 7.5 and 150 mM NaCl. The peak fractions were collected and concentrated. The purified samples were analyzed by SDS-gel electrophoresis and then frozen by liquid nitrogen, and stored at -80°C before use. All steps were performed either in cold storage or on ice.

Pull-down assays

100 μg of His-tagged ABCA7/ABCC3 was mixed with 10-fold molar excess of ApoE3. The buffer containing 50 mM Tris pH 7.5, 150 mM NaCl and 0.02% (w/v) GDN was added to the mixture up to 2 mL. The mixture was then incubated at 4°C with gentle rotation for 3 hr. After that, the mixture was loaded onto a Ni-NTA resin (Cytiva) and incubated on ice for 2 hr with gentle agitation. Then the resin was washed with 100 mL wash buffer containing 50 mM Tris-HCl pH 7.5, 150 mM NaCl, and 0.02% (w/v) GDN. The protein was eluted with 6 mL of elution buffer containing 50 mM Tris-HCl pH 7.5, 150 mM NaCl, 300mM Imidazole and 0.02% (w/v) GDN. Finally, the eluent was concentrated and analyzed by SDS-gel electrophoresis.

Lipid preparation

Lipids used in the ATPase activity assays and lipid transport activity assays, including dioleoylphosphatidylserine (DOPS), dioleoylphosphatidylcholine (DOPC), dioleoylphosphatidylethanolamine (DOPE), 1-stearoyl-2-oleoyl-sn-glycero-3-phospho-L-serine (SOPS), 1,2-Dipalmitoyl-sn-glycero-3-phospho-L-serine (DPPS), 1,2-dimyristoyl-sn-glycero-3-phospho-L-serine (DMPS), porcine brain polar lipid (BPL), [7-nitro-2-1,3-benzoxadiazol-4-yl)amino]hexanoyl-sn-glycero-3-phosphoserine (NBD-PS), [7-nitro-2-1,3-benzoxadiazol-4-yl)amino]hexanoyl-sn-glycero-3-phosphoethanolamine (NBD-PE) and [7-nitro-2-1,3-benzoxadiazol-4-yl) amino]hexanoyl-sn-glycero-3-phosphocholine (NBD-PC) were purchased from Avanti. All lipids were prepared in chloroform and dried under N_2. Then they were dissolved in the buffer containing 50 mM Tris-HCl pH 7.5, 150 mM NaCl to a final concentration of 10 mg/mL. After sonication for 30 min and 3 freeze-thaw cycles, all lipids were stored at -20°C before use.

ATPase activity assays

The ATPase activities of wild-type ABCA7 and all mutants in the detergent were measured using an ATPase colorimetric Assay Kit (Innova Biosciences) in 96-well plates at $OD_{630\ nm}$.

For the substrate-stimulated ATPase activity assay, protein at a final concentration of 0.1 μM was added to the reaction buffer containing 50 mM Tris-HCl pH 7.5, 150 mM KCl, 0.02% (w/v) GDN and 10 mM $MgCl_2$. Then, each substrate was added into the reaction mixture with a final concentration of 300 μM. As for ATPase activity assay of ABCA7 with ApoE, the concentration of ApoE was 1 μM. The mixture was incubated on the ice for 10 min, then ATP (Sigma) was supplemented in the solution with a final concentration of 2 mM. Reactions were performed at 37°C for 30 min, and the amount of released phosphate group (Pi) was quantitatively measured using a SpectraMax iD5 Multi-Mode Microplate Reader (Molecular Devices). The control groups in the absence of proteins were subtracted as background for each data point. Data are presented as the means ± SD by biological repeats from three independent assays (n = 3).

Proteoliposome-based phosphatidylserine transport assay

Lipid mixtures (99.4% BPL and 0.6% NBD-PS) were prepared in chloroform and dried under N_2. Then the lipids were resuspended in buffer containing 50 mM Tris-HCl pH 7.5 and 150 mM NaCl to the final concentration of 10 mg/mL. As one reaction sample, lipids were extruded 21 times and treated by 0.45% Triton X-100 for 1 hr at room temperature. Then ABCA7 preincubated with or without 10 μg ApoE was added to the destabilized liposomes and incubated for 1 hr at 4°C. The ratio of lipids and proteins was kept at 80:1 (wt/wt). Triton X-100 was then removed by incubation with 400 mg SM-2 Adsorbent Bio-Beads (Bio-Rad) per mL reaction mixture overnight at 4°C. The suspension was centrifuged at 250,000 × g for 1 hr at 4°C. The liposome suspension was removed, and the liposomal pellet was washed once with reconstitution buffer containing 50 mM Tris-HCl pH 7.5, 150 mM KCl and 10 mM $MgCl_2$. The suspension was then centrifuged at 250,000 × g for 30 min at 4°C to remove the supernatant and resuspended in

reconstitution buffer at a final concentration of 0.1 μM for transport activity assays. The treated proteoliposomes were stored at 4°C before use.

For each individual measurement, 40 μL of proteoliposomes were incubated with 2 mM ATP in the presence or absence of 10 mM $MgCl_2$ in 10 μL of reaction buffer containing 50 mM Tris-HCl pH 7.5, 150 mM KCl for 20 min at 37°C. After incubation, each sample was diluted to 100 μL with reaction buffer and assayed for probe distribution. The fluorescence (FT) was recorded continuously in a CLARIOstar fluorometer (BMG LABTECH, Inc.) (λ_{ex} = 485 nm, λ_{em} = 520 nm). After stable baseline was obtained, 10 μL of 50 mM dithionite dissolved in 1 M Tris HCl (pH 10) was added to the sample and mixed to quench the fluorescent probes in the outer leaflet of liposomes, and fluorescence (FD) was recorded until a stable line was obtained. Subsequently, the sample was solubilized by the addition of 10 μL of 10% Triton X-100, and the background fluorescence (FO) was recorded for another 180 s. The percentage of NBD-PS in the outer leaflet of proteoliposomes that is accessible to dithionite quenching was calculated as (FT-FD)/(FT-FO) × 100%.

Cryo-EM sample preparation and data collection

The purified protein was concentrated to ~6.5 mg/mL. An aliquot of 3.5 μL of the samples was applied to glow-discharged Quantifoil R1.2/1.3 300-mesh Cu Holey Carbon Grids. Then the grids were blotted for 3.5 s with a blot force 0, and then plunged into liquid ethane using a Vitrobot Mark IV (FEI) at 4°C and 100% humidity.

The cryo-EM data of apo-form ABCA7 (E965Q/E1951Q) were collected with EPU2 software on a Titan Krios microscope at 300 kV equipped with a K3 detector (Gatan) and a GIF Quantum energy filter (Gatan), at the Center for Integrative Imaging, University of Science and Technology of China (USTC). A total of 2,013 micrographs were collected in super-resolution mode at a nominal magnification of 81,000× with defocus values from -2.5 to -1.5 μm. Each movie stack of 32 frames was exposed a total dose of ~55 $e^- Å^{-2}$.

The cryo-EM data of lipid-bound ABCA7 were collected at the Center for Biological Imaging at the Institute of Biophysics (IBP), Chinese Academy of Sciences (CAS). A total of 3,784 micrographs were collected in super-resolution mode with a K3 camera at nominal magnification of 22,500× with a defocus range from -2.0 to -1.5 μm. Each movie stack of 32 frames was exposed a total dose of ~60 $e^- Å^{-2}$.

For all of these stacks, motion correction and dose weighting were performed with patch motion correction with a Fourier cropping factor of 0.535, resulting in a pixel size of 1.07. Meanwhile, the defocus values were estimated using Patch CTF estimation.[65]

Cryo-EM data processing

For the apo-form ABCA7 datasets, after manual removal of bad micrographs, a total of 1,213,428 particles were automatically picked in cryoSPARC 3.2.[65] These particles were then subjected to 2D classification and particles of the best classes were re-extracted for further data processing. A total of 1,059,691 particles with structural features were extracted and subjected to ab-initial reconstruction and heterogeneous refinement, during which particles were classified into 3 classes. 44,853 particles from the best classes were merged together and subjected to non-uniform refinement and local refinement with an adapted mask. After refinement, selected particles generated an EM map with an overall resolution of 3.9 Å (Figure S2).

For the lipid-bound ABCA7 datasets, 2,317,868 particles were picked out by reference-based auto-pick and subjected to 2D classification. Then 1,909,642 particles were selected and subjected to ab-initial reconstruction and heterogeneous refinement. Afterwards, A total of 473,349 particles from the best class were further subjected to non-uniform refinement and local refinement, resulting in a final map at 3.5 Å resolution (Figure S5).

Model building and refinement

The final sharpened map was used for model building in Coot 0.9.5.[70] A homology model of apo-form ABCA7 was generated by SWISS-MODEL server,[71] using the structure of human ABCA1 (PDB code 5XJY) as the reference and corrected based on the structure of human ABCA7 predicted by *AlphaFold2*. The ABC core part can be built well according to the template model in COOT, but the electron density of NBD2 and RD does not match it obviously. Although EM map of NBD2 and RD revealed very poor density, the quality of density allowed rigid-body placement for the entire domain based on a homology model of the structure in ABCA1 and ABCA4 (PDB code 7E7I). After several rounds of manual building, the model was almost completely built and automatically refined against the map by the real_space_refine program in PHENIX[68] with secondary structure and geometry restraints. The final model contains residues Phe3-Ala135, Gln177-Cys225, Ser264-Leu352, Glu371-Pro443, Gln460-Gly760, Lys793-Ala1040, Val1073-Cys1150, Trp1214-Glu1757 and Gln1774-Asp2103.

The apo-form structure of ABCA7 was used as the reference for model building of lipid-bound ABCA7. After manually adjusted of side-chains as allowed for the map, the model was refined and validated by PHENIX and COOT. Two extra asymmetric densities between TMD1 and TMD2 can be observed, each of which was fitted by a DOPS molecule (PDB code 17F). The final model contains residues Met1-Ala135, Ala176-Val227, Ser264-Met354, Phe376-Pro443, Pro459-Gly770Arg, Leu824-Lys1039, Arg1072-Ala1151, Trp1214-Pro1759, Val1792-Leu1798 and Arg1812-Gln2104.

The model refinement and validation statistics were summarized in Table S2. The programs of UCSF Chimera, ChimeraX and PyMOL (The PyMOL Molecular Graphics System, Version 2.5.2 Copyright (C) Schrödinger, LLC.) were used for preparing the structural figures. Protein sequences were aligned using Multalin (http://multalin.toulouse.inra.fr/multalin/), and the sequence-alignment figures were generated by ESPript3 server (https://espript.ibcp.fr/).

Please cite this article in press as: Fang et al., Structural insights into human ABCA7-mediated lipid transport, Structure (2024), https://doi.org/10.1016/j.str.2024.12.015

QUANTIFICATION AND STATISTICAL ANALYSIS

To quantify the ATPase activity and the phospholipid transport efficiency, mean values and the standard deviation from at least three independent measurements were calculated. The half maximum effective concentration of phospholipid and the maximum ATPase activity of ABCA7 were determined by nonlinear regression of the Michaelis-Menten equation using OriginPro. The specific ATP turnover rates were calculated assuming a molecular weight of 234 kDa for ABCA7.

The orientation distribution of the particles used in the final reconstruction and the local resolution map was calculated using cryoSPARC3.2. Resolution estimations of cryo-EM density maps are based on the 0.143 Fourier shell correlation criterion (Kucukelbir et al., 2014).

The multiple sequence alignments were performed by MultAlin (http://multalin.toulouse.inra.fr/multalin/).

Cryo-EM data collection and refinement statistics are summarized in Table S2.